Threshold of Parametric Instability in the Ionospheric Heating Experiments

Xiang WANG (王翔)[1,2], Chen ZHOU (周晨)[1,*], Moran LIU (刘默然)[1], Farideh HONARY[2], Binbin NI (倪彬彬)[1], Zhengyu Zhao (赵正予)[1]

[1]Department of Space Physics, School of Electronic Information, Wuhan University, Wuhan, 430072, People's Republic of China

[2]Department of Physics, Lancaster University, Lancaster, LA1 4YB, United Kingdom

[*]Corresponding author: chenzhou@whu.edu.cn

Abstract

Many observations in the ionospheric heating experiment, by a powerful high frequency electromagnetic wave with ordinary polarization launched from a ground-based facility, is attributed to parametric instability (PI). In this paper, the general dispersion relation and the threshold of the PI excitation in the heating experiment are derived by considering the inhomogeneous spatial distribution of pump wave field. It is shown that the threshold of PI is influenced by the effective electron and ion collision frequencies and the pump wave frequency. Both collision and Landau damping should be considered in the PI calculation. The derived threshold expression has been used to calculate the required threshold for excitation of PI for several ionospheric conditions during heating experiments conducted employing EISCAT high frequency transmitter in Tromsø, Norway on October 2nd 1998, November 8th 2001, October 19th 2012 and July 7th 2014. The results indicate that the calculated threshold is in good agreement with the experimental observations.

Keywords: ionospheric plasma, ionospheric modification; parametric instability; ordinary polarized EM wave

1 Introduction

Ionospheric modification experiments, by high powerful high-frequency electromagnetic waves launched from the ground heating facilities, have observed many nonlinear plasma instabilities in the past decades [1-7]. Parametric instability is directly or indirectly employed to explain the observed phenomena during the heating experiments, such as high-frequency enhanced ion line (HFILs), high-frequency enhanced plasma line (HFPLs) [8, 9], airglow enhancement [10-12], stimulated electromagnetic emissions (SEEs) [13], filed-aligned irregularities (FAIs) [14, 15], etc.

The excitation process of plasma instabilities includes a multi-wave coupling process [7, 16-20]. Two waves in the ionosphere can interact, causing perturbations to the parameters such as current and charge density. These effects can be associated with frequency differences or frequency sums of the two waves. Whilst a third wave, or even a fourth wave, whose frequency equals the frequency difference or sum and whose wave vector meets the requirement of the vector difference or sum, can be excited in the ionosphere. Ion acoustic wave/lower hybrid wave/zero-frequency density irregularities and the Langmuir wave/upper hybrid wave are example wave modes exist in the ionospheric plasma; an incident high power radio wave can interact with any of these wave modes when the matching conditions of frequency and wave vectors are satisfied.

Theoretical research of parametric instabilities in space plasma began in the 1950s by considering nonlinear theory of wave mode transition when a Langmuir wave can decay to another Langmuir wave and an ion acoustic wave under certain conditions [21], and Silin [22, 23],

who first systematically studied the process of coupling and excitation of waves in the process of parametric instability, started from the collisionless, cold plasma fluid equations, which were adopted only when the field strength of the incident pump wave is stronger than the threshold field. Nishikawa [24, 25] studied the general model of exciting parameter instabilities and analyzed the excitation of plasma waves under three conditions: (1) $\omega_1+\omega_2 \approx \omega_0$, (2) $\omega_1 << \omega_2 \lesssim \omega_0$, (3) $\omega_1 << \omega_0 \lesssim \omega_2$. His results showed that the waves excited by (1) and (2) are oscillating and that the wave of excited by (3) is non-oscillating. The equality of the threshold field can be obtained from different methods, e.g., using the plasma hydrodynamic equations [7, 18, 24, 25], or Vlasov equation [17, 26]. The differences between these methods are small, and they all show proportional relation between the square of the threshold field intensity and the electron collision frequency. Based on numerical simulations, Guzdar et al. [27] calculated the threshold field strength of the pump wave that excites the parametric instability irregularly and found that this threshold field strength can reach 10 V/m. Recently, Kuo [7, 18, 19] obtained a different expression and illustrated that the square of threshold field strength is proportional to the product of the electron and ion collision frequencies.

In this paper, MHD equations are employed to derive the parametric excitation in the ionospheric heating experiment by a high powerful high-frequency ordinary polarized electromagnetic wave. Equations presented here consider inhomogeneous spatial distribution of pump wave field as well as Landau damping of Langmuir wave. In section 2, parametric excitation in the ionosphere and its dispersion relation, as well as the dispersion relation of the excited high frequency sidebands and the low frequency decay mode are calculated when the inhomogeneous spatial distribution of pump wave field is included. Our method for calculating the

instability threshold indicates that both collision and Landau damping terms are needed to explain the experimental observations in section 3, followed by the conclusion and summary in section 4.

2 Theory

2.1 Excitation of parametric instability

Ionospheric heating experiments have shown that Langmuir waves/upper hybrid wave and ion acoustic waves/lower hybrid wave can be excited in the ionospheric modification [7, 9, 28, 29]. The pump wave $\vec{E}_{\mathrm{p}}\left(\vec{k}_0, \omega_0\right)$ could be either an electromagnetic (EM) wave or an electrostatic (ES) wave. It was hypothesized that the oscillations of the main modes in the plasma are $\left(\pm k, \pm\omega\right)$ and, $\left(k_{\mathrm{d}} = \Delta k, \omega_{\mathrm{d}} = \Delta\omega\right)$, In general, this excitation process includes a four-wave coupling process; which it will reduce to a three-wave coupling process under certain conditions. This process requires a wave vector and frequency matching condition:

$$\omega_0 = \omega_+ + \omega_{\mathrm{d}} = \omega_- - \omega_{\mathrm{d}} \tag{1}$$

$$\vec{k}_0 = \vec{k}_+ + \vec{k}_{\mathrm{d}} = \vec{k}_- - \vec{k}_{\mathrm{d}} \tag{2}$$

where the subscripts 0, +, - and d represent the pump wave, the down-shifted high frequency mode, the up-shifted high frequency mode and the low frequency decay mode, respectively.

The dispersion relation for the parametric instability is derived from the following equations:

Continuity Equation

$$\partial n_\alpha / \partial t + \nabla \cdot \left(n_\alpha v_\alpha\right) = 0 \tag{3}$$

Momentum Equations:

$$m_{\mathrm{e}} n_{\mathrm{e}} \left(\partial/\partial t + \vec{v}_{\mathrm{e}} \cdot \partial/\partial r\right)\vec{v}_{\mathrm{e}} = -e n_{\mathrm{e}} \left(\vec{E} + \vec{v}_{\mathrm{e}} \times \vec{B}\right) + e n_{\mathrm{e}} \nabla\Phi - 3T_{\mathrm{e}} \nabla \delta n_{\mathrm{e}} - m_{\mathrm{e}} n_{\mathrm{e}} \upsilon_{\mathrm{e}} \vec{v}_{\mathrm{e}} \tag{4a}$$

$$m_{\mathrm{i}} n_{\mathrm{i}} \left(\partial/\partial t + \vec{v}_{\mathrm{i}} \cdot \partial/\partial r\right)\vec{v}_{\mathrm{i}} = e_{\mathrm{i}} n_{\mathrm{i}} \left(\vec{E} + \vec{v}_{\mathrm{i}} \times \vec{B}\right) - e_{\mathrm{i}} n_{\mathrm{i}} \nabla\Phi - T_{\mathrm{i}} \nabla \delta n_{\mathrm{i}} + m_{\mathrm{i}} n_{\mathrm{i}} \upsilon_{\mathrm{i}} \vec{v}_{\mathrm{i}} \tag{4b}$$

Poisson Equation

$$\nabla^2\Phi = -\sum e_\alpha n_\alpha \big/ \varepsilon_0 \tag{5}$$

where the subscript α refers to e and i, the electron and ion, respectively. n_α, m_α, e_α, T_α and $\vec{v}_\alpha$ are the density, mass, charge, temperature, and speed of particle α, respectively. $\vec{E}$ is the electric field strength; $\vec{B}$ is the magnetic field; Φ is the potential of the plasma wave; ε_0 is the free space permittivity; and electron and ion effective collision frequencies are given by $\upsilon_\mathrm{e} = \upsilon_\mathrm{ei} + \upsilon_\mathrm{en} + \upsilon_\mathrm{eL}$ and $\upsilon_\mathrm{i} = \upsilon_\mathrm{ie} + \upsilon_\mathrm{in} + \upsilon_\mathrm{iL}$, respectively, where υ_ei, υ_en, υ_eL, υ_ie υ_in and υ_iL are electron-ion collision frequency, electron-neutral collision frequency, electron Landau damping rate, ion-electron collision frequency, ion-neutral collision frequency and ion Landau damping rate, respectively.

The incident pump wave field is assumed to be:

$$\vec{E} = \vec{E}_{\mathrm{k}_0} \exp\left[i\left(\vec{k}_0 \cdot \vec{r} - \omega_0 t\right)\right] \big/ 2 \tag{6}$$

The perturbation of the incident pump field is assumed to be small, meaning that the magnitude of the intensity of the excited plasma waves is far less than that of the pump wave. The density of charged particles satisfies the quasi-neutrality condition, i.e. $n_0^\mathrm{e} = n_0^\mathrm{i} = \text{constant}$. Every physical quantity is treated as the sum of frequency components, for example, $\vec{v} = \vec{v}_{(\mathrm{k}_0,\omega_0)} + \vec{v}_{(\pm\mathrm{k},\pm\omega)} + \vec{v}_{(\Delta\mathrm{k},\Delta\omega)}$, where the subscript is the exponent, likewise, $\vec{v}_{(\pm\mathrm{k},\pm\omega)} = \vec{v}_\mathrm{k} \exp\left[i\left(\vec{k}\cdot\vec{r} - \omega t\right)\right] + \vec{v}_{-\mathrm{k}} \exp\left[-i\left(\vec{k}\cdot\vec{r} - \omega t\right)\right]$. The physical quantities described by frequency components are incorporated into the original equations and the terms of the same exponent are combined. The arbitrariness of $\vec{r}$ and t demands that the coefficient of each exponent term is equal to zero. Thus, a series of equations of frequency components can be obtained to determine the dispersion relation of the wave coupling. Finally, the excitation condition of the parametric instability can be acquired by analyzing the dispersion relation

equation.

To begin with, let us consider the geomagnetic field $\vec{B}_0 = B_0\hat{z}$ and the wave number k_0 of the heater wave is much smaller than the wave numbers of the electrostatic, i.e. $k_0 \approx 0$. First of all, we simplify the equations concerning the $(+k_0, +\omega_0)$ wave mode. The momentum equation can be reduced to:

$$\left(\frac{\partial}{\partial t} + \upsilon_e\right)\vec{V}_{k_0} + \Omega_e\vec{V}_{k_0} \times \hat{z} = -\frac{e}{2m_e}\vec{E}_{k_0} \tag{7}$$

The cross product of the k_0 component of Eq. (7) with $\hat{z}$ is taken as:

$$\left(\frac{\partial}{\partial t} + \upsilon_e\right)\left(\vec{V}_{k_0} \times \hat{z}\right) - \Omega_e\vec{V}_{k_0\perp} = -\frac{e}{2m_e}\vec{E}_{k_0} \times \hat{z} \tag{8}$$

Take the perpendicular component of Eq. (7) into Eq. (8),

$$\left[\left(\frac{\partial}{\partial t} + \upsilon_e\right)^2 + \Omega_e^2\right]\left(\vec{V}_{k_0} \times \hat{z}\right) = -\Omega_e\frac{e}{2m_e}\vec{E}_{k_0\perp} - \left(\frac{\partial}{\partial t} + \upsilon_e\right)\frac{e}{2m_e}\vec{E}_{k_0} \times \hat{z} \tag{9}$$

Substitute Eq. (9) into Eq. (7)

$$\begin{aligned}&\left(\frac{\partial}{\partial t} + \upsilon_e\right)\left[\left(\frac{\partial}{\partial t} + \upsilon_e\right)^2 + \Omega_e^2\right]\vec{V}_{k_0} = \\ &-\frac{e}{2m_e}\left[\left(\frac{\partial}{\partial t} + \upsilon_e\right)^2\vec{E}_{k_0} + \Omega_e^2\vec{E}_{k_0 z} - \Omega_e\left(\frac{\partial}{\partial t} + \upsilon_e\right)\vec{E}_{k_0} \times \hat{z}\right]\end{aligned} \tag{10}$$

Equation (10) can be written as a scalar equation in the $k-\omega$ domain to obtain the expression of $\vec{V}_{k_0}$:

$$\vec{V}_{k_0} = -i\frac{e\left[(\omega_0 + i\upsilon_e)^2\vec{E}_{k_0} - \Omega_e^2\vec{E}_{k_0 z} - i(\omega_0 + i\upsilon_e)\Omega_e\vec{E}_{k_0} \times \hat{z}\right]}{2m_e(\omega_0 + i\upsilon_e)\left[(\omega_0 + i\upsilon_e)^2 - \Omega_e^2\right]} \tag{11}$$

where $\Omega_e = eB_0/m_e$ is the electron cyclotron frequency.

In the high frequency sideband wave field, only electron can respond to the wave field due to its small inertia. To use the same procedure to treat $(\pm k, \pm\omega)$ component the dispersion relation

of the high frequency sideband plasma wave excited by parametric instability can be obtained

$$\begin{aligned}
&\left[\left(\omega+i\upsilon_{\mathrm{e}}\right)^2-\Omega_{\mathrm{e}}^2\right]\left(\omega^2+i\upsilon_{\mathrm{e}}\omega-3k^2v_{\mathrm{Te}}^2-\omega_{\mathrm{pe}}^2-\Omega_{\mathrm{e}}^2\sin^2\theta\right)n_{\pm\mathrm{k}} \\
&=\frac{e^2}{m_{\mathrm{e}}^2}\left\{\begin{array}{l}
+\dfrac{\left[-\left(\omega+i\upsilon_{\mathrm{e}}\right)^2+\Omega_{\mathrm{e}}^2\cos^2\theta\right]}{\left(\omega_0^2+\upsilon_{\mathrm{e}}^2\right)^2\left(\omega_0^2+\upsilon_{\mathrm{e}}^2-\Omega_{\mathrm{e}}^2\right)^2}\cdot\left\{\begin{array}{l}\left(\omega_0^2+\upsilon_{\mathrm{e}}^2\right)^2\left(\vec{k}\cdot\vec{E}_{\mathrm{p}}\right)^2+\Omega_{\mathrm{e}}^4\left(\vec{k}\cdot\vec{E}_{\mathrm{pz}}\right)^2\\+\left(\omega_0^2+\upsilon_{\mathrm{e}}^2\right)\Omega_{\mathrm{e}}^2\left(\vec{k}\cdot\vec{E}_{\mathrm{p}}\times\hat{z}\right)^2\end{array}\right\}\\
+\dfrac{i\Omega_{\mathrm{e}}\left(\omega+i\upsilon_{\mathrm{e}}\right)}{\left(\omega_0^2+\upsilon_{\mathrm{e}}^2\right)^2\left(\omega_0^2+\upsilon_{\mathrm{e}}^2-\Omega_{\mathrm{e}}^2\right)^2}\left\{\begin{array}{l}\left(\omega_0^2+\upsilon_{\mathrm{e}}^2\right)^2\left(\vec{k}\cdot\vec{E}_{\mathrm{p}}\times\hat{z}\right)\left(\vec{k}\cdot\vec{E}_{\mathrm{p}}^{*}\right)\\+\left(\omega_0^2+\upsilon_{\mathrm{e}}^2\right)\Omega_{\mathrm{e}}^2\left(\vec{k}\cdot\vec{E}_{\mathrm{p}}\times\hat{z}\right)\left(-\vec{k}\cdot\vec{E}_{\mathrm{p}\perp}^{*}\right)\end{array}\right\}
\end{array}\right\}n_{\pm\mathrm{k}} \\
&\pm i\frac{e}{2m_{\mathrm{e}}}\left\{\left[\left(-i\omega+\upsilon_{\mathrm{e}}\right)^2\vec{k}+\Omega_{\mathrm{e}}^2\vec{k}_{\mathrm{z}}\right]\cdot\vec{E}_{\mathrm{k}_0}-\Omega_{\mathrm{e}}\left(-i\omega+\upsilon_{\mathrm{e}}\right)\vec{k}\cdot\vec{E}_{\mathrm{k}_0}\times\hat{z}\right\}n_{\pm\Delta\mathrm{k}}
\end{aligned}\qquad(12)$$

where $\omega_{\mathrm{pe}}^2=\left(n_0e^2/\varepsilon_0m_{\mathrm{e}}\right)$, $v_{\mathrm{T_e}}^2=\left(k_{\mathrm{b}}T_{\mathrm{e}}/m_{\mathrm{e}}\right)$ are the electron plasma frequency, and the electron thermal speed, respectively and k_{b} is the Boltzmann constant. The term in the left-hand side of Eq. (12) defines the dispersion relation of the excited high frequency plasma wave; while the terms in the right-hand side are the coupling terms driving the plasma waves. The first term in the right-hand side is caused by the spatial non-uniformity of the wave field and the second term indicates the coupling between the pump wave and the lower frequency decay mode, which influences the excitation of the high frequency Langmuir wave/ upper hybrid wave sideband. The ratio of the two terms in the right-hand side of Eq. (12) is close to 1; which indicates that the nonlinear force generated by the non-uniform spatial wave field is important in the excitation of parametric instability.

Finally, the dispersion relation of the low frequency decay mode can be analyzed in the following manner. Both the electron and the ion contribute to the low frequency plasma wave field. For simplification, electrons and ions assume to maintain quasi-neutrality in the low frequency plasma wave field, i.e. $n_{\Delta\mathrm{k}}^{\mathrm{i}}\approx n_{\Delta\mathrm{k}}^{\mathrm{e}}=n_{\Delta\mathrm{k}}$. This results in a scalar equation:

$$\left\{\begin{array}{l}-\left[-\left(\Delta\omega+i\upsilon_{\mathrm{e}}\right)^2+\Omega_{\mathrm{e}}^2\right]\left[-\Delta\omega\left(\Delta\omega+i\upsilon_{\mathrm{i}}\right)+k^2c_{\mathrm{s}}^2\right]\cos^2\theta \\ -\Delta\omega\left(\Delta\omega+i\upsilon_{\mathrm{i}}\right)\sin^2\theta\left[\left(\Delta\omega+i\upsilon_{\mathrm{e}}\right)^2\left(1+\cot^2\theta\right)-k^2c_{\mathrm{s}}^2-\Omega_{\mathrm{e}}\Omega_{\mathrm{i}}\left(1+\frac{m_{\mathrm{i}}}{m_{\mathrm{e}}}\cot^2\theta\right)\right]\end{array}\right\}n_{\pm\Delta\mathrm{k}}=$$

$$-\frac{m_{\mathrm{e}}}{m_{\mathrm{i}}}\left\{\begin{array}{l}+\dfrac{\left[-\left(\omega+i\upsilon_{\mathrm{e}}\right)^2+\Omega_{\mathrm{e}}^2\cos^2\theta\right]}{\left(\omega_0^2+\upsilon_{\mathrm{e}}^2\right)^2\left(\omega_0^2+\upsilon_{\mathrm{e}}^2-\Omega_{\mathrm{e}}^2\right)^2}\left\{\begin{array}{l}\left(\omega_0^2+\upsilon_{\mathrm{e}}^2\right)^2\left(\vec{k}\cdot\vec{E}_{\mathrm{p}}\right)^2+\Omega_{\mathrm{e}}^4\left(\vec{k}\cdot\vec{E}_{\mathrm{pz}}\right)^2 \\ +\left(\omega_0^2+\upsilon_{\mathrm{e}}^2\right)\Omega_{\mathrm{e}}^2\left(\vec{k}\cdot\vec{E}_{\mathrm{p}}\times\hat{z}\right)^2\end{array}\right\} \\ +\dfrac{i\Omega_{\mathrm{e}}\left(\omega+i\upsilon_{\mathrm{e}}\right)}{\left(\omega_0^2+\upsilon_{\mathrm{e}}^2\right)^2\left(\omega_0^2+\upsilon_{\mathrm{e}}^2-\Omega_{\mathrm{e}}^2\right)^2}\left\{\begin{array}{l}\left(\omega_0^2+\upsilon_{\mathrm{e}}^2\right)^2\left(\vec{k}\cdot\vec{E}_{\mathrm{p}}\times\hat{z}\right)\left(\vec{k}\cdot\vec{E}_{\mathrm{p}}^*\right) \\ +\left(\omega_0^2+\upsilon_{\mathrm{e}}^2\right)\Omega_{\mathrm{e}}^2\left(\vec{k}\cdot\vec{E}_{\mathrm{p}}\times\hat{z}\right)\left(-\vec{k}\cdot\vec{E}_{\mathrm{p}\perp}^*\right)\end{array}\right\}\end{array}\right\}n_{\pm\Delta\mathrm{k}}$$

$$+\frac{m_{\mathrm{e}}}{m_{\mathrm{i}}}\left\{\begin{array}{l}\left[-\left(\Delta\omega+i\upsilon_{\mathrm{e}}\right)^2+\Omega_{\mathrm{e}}^2\sin\theta\right]\left[n_0\left(\vec{k}\cdot\vec{V}_{\mathrm{k}_0}\right)\left(\vec{k}\cdot\vec{V}_{\pm\mathrm{k}}\right)\right]-i\Omega_{\mathrm{e}}\left(\Delta\omega+i\upsilon_{\mathrm{e}}\right)\left[n_0\left(\vec{k}\cdot\vec{V}_{\mathrm{k}_0}\right)\left(\vec{k}\cdot\vec{V}_{\pm\mathrm{k}}\right)\times\hat{z}\right] \\ +\left(\Delta\omega+i\upsilon_{\mathrm{e}}\right)\left[-\left(\Delta\omega+i\upsilon_{\mathrm{e}}\right)^2+\Omega_{\mathrm{e}}^2\right]\left(\mp\vec{k}\cdot\vec{V}_{\mathrm{k}_0}\right)n_{\pm\mathrm{k}} \\ +\dfrac{en_{\pm\mathrm{k}}}{2m_{\mathrm{e}}}\left[-\left(\Delta\omega+i\upsilon_{\mathrm{e}}\right)^2+\Omega_{\mathrm{e}}^2\cos^2\theta+i\Omega_{\mathrm{e}}\left(\Delta\omega+i\upsilon_{\mathrm{e}}\right)\sin^2\theta\right]\left(\pm i\vec{k}\cdot\vec{E}_{\mathrm{k}_0}\right)\end{array}\right\} \tag{13}$$

where $c_{\mathrm{s}}^2=k_{\mathrm{b}}\left(T_{\mathrm{e}}+3T_{\mathrm{i}}\right)/m_{\mathrm{i}}$ is the ion acoustic wave phase speed, $\Omega_{\mathrm{i}}=eB_0/m_{\mathrm{i}}$ is the ion cyclotron frequency, θ is the angle between the wave vector $\vec{k}$ and the magnetic field $\vec{B}_0$; $\vec{V}_{\pm\mathrm{k}}=+\dfrac{e\left\{\left(\upsilon_{\mathrm{e}}-i\omega\right)^2\nabla+\Omega_{\mathrm{e}}^2\nabla_{\mathrm{z}}-\left(\upsilon_{\mathrm{e}}-i\omega\right)\Omega_{\mathrm{e}}\nabla\times\hat{z}\right\}}{m_{\mathrm{e}}\left(\upsilon_{\mathrm{e}}-i\omega\right)\left[\left(\upsilon_{\mathrm{e}}-i\omega\right)^2+\Omega_{\mathrm{e}}^2\right]}\dfrac{en_{\pm\mathrm{k}}}{\varepsilon_0k^2}$, which is the linear part of the electron velocity response to the high frequency plasma wave field. The terms in the left-hand side of Eq. (13) defines the dispersion relation of the excited low frequency decay mode in the parametric instability. The right-hand side of Eq. (13) illustrates the coupling terms driven the parametric instability. The pump wave and the high frequency sidebands couple with each other to exert a low frequency nonlinear force on electrons and to make the coupling waves grow significantly in the expense of the pump wave.

2.2 Instability Threshold

In this section, excitation of parametric instability by an ordinary polarized electromagnetic pump wave in the ionospheric modification experiments is considered. In this condition, the O-mode pump wave $\vec{E}_{\mathrm{p}}\left(\vec{k}_0,\omega_0\right)$ decays to a Langmuir/upper hybrid sideband $n_{\pm\mathrm{k}}\left(\pm\vec{k},\omega_{\pm}\right)$ and an ion acoustic wave mode/purely growing mode/ lower hybrid mode $n_{\Delta\mathrm{k}}\left(\Delta\vec{k},\Delta\omega\right)$ below

the reflection height of the pump wave. In terms of the wave frequency and wave vector matching condition, i.e. Eq. (1) and (2), the following expression of the frequency and wave vector are obtained: $\omega_{\pm} = \omega = \omega_0 - \Delta\omega$, $\vec{k}_{+} = -\vec{k}_{-} = -\Delta\vec{k}$, where

$$\vec{k} = k_z \hat{z} + k_{\perp} \hat{x} \tag{14}$$

The pump wave field can be expressed as

$$\vec{E}_{\mathrm{p}} = \hat{z}\, E_{\mathrm{k}_0} / 2 + \left(\hat{x} + i\hat{y}\right) E_{\mathrm{k}_0} / 2 \tag{15}$$

In the following, Eq. (12) and (13) with the aid of Eq. (14) and (15) are analyzed to explain excitation of parametric instabilities for different scenarios.

2.2.1 Parametric instability near the O-mode wave reflection height

When the ordinary polarized EM wave propagates to the region near the reflection altitude, the electric field of the pump wave is $\vec{E}_{\mathrm{p}} = \hat{z}\left(E_{\mathrm{k}_0}/2\right)\cos\left(-i\omega_0 t\right)$. Then the expressions for $\vec{V}_{\mathrm{k}_0}$, $\vec{V}_{\pm\mathrm{k}}$, $\left(\vec{k}\cdot\vec{V}_{\mathrm{k}_0}\right)\cdot\left(\vec{k}\cdot\vec{V}^{*}_{\pm\mathrm{k}}\right)$, and $\left(\vec{k}\cdot\vec{V}_{\mathrm{k}_0}\right)\cdot\left(\vec{k}\cdot\vec{V}^{*}_{\mathrm{k}_0}\right)$ reduce to

$$\vec{V}_{\mathrm{k}_0} = i\frac{e\vec{E}_{\mathrm{k}_0}}{2m_{\mathrm{e}}\left(\omega_0 + i\upsilon_{\mathrm{e}}\right)} \tag{16a}$$

$$\vec{V}_{\pm\mathrm{k}} = \mp\frac{\vec{k}\,\omega_{\mathrm{pe}}^2}{k^2\left(\omega + i\upsilon_{\mathrm{e}}\right)}\frac{n_{\pm\mathrm{k}}}{n_0} \tag{16b}$$

$$\left(\vec{k}\cdot\vec{V}_{\mathrm{k}_0}\right)\cdot\left(\vec{k}\cdot\vec{V}^{*}_{\mathrm{k}_0}\right) = \frac{e^2\left(\vec{k}\cdot\vec{E}_{\mathrm{k}_0}\right)^2}{4m_{\mathrm{e}}^2\left(\omega_0^2 + \upsilon_{\mathrm{e}}^2\right)} \tag{16c}$$

$$\left(\vec{k}\cdot\vec{V}_{\mathrm{k}_0}\right)\left(\vec{k}\cdot\vec{V}^{*}_{\pm\mathrm{k}}\right) = \mp i\frac{e\omega_{\mathrm{pe}}^2\vec{k}\cdot\vec{E}_{\mathrm{k}_0}}{2m_{\mathrm{e}}\left(\omega_0^2 + \upsilon_{\mathrm{e}}^2\right)}\frac{n_{\pm\mathrm{k}}}{n_0} \tag{16d}$$

Considering a case when the pump wave decay to a Langmuir wave and an ion acoustic wave, the process reduces to a three-wave interaction, i.e. a pump wave, a Langmuir wave and an ion acoustic wave are involved in the coupling process. The dispersion relation reduces to

$$\begin{aligned}&\left\{\left(-\omega^2-i\upsilon_{\mathrm{e}}\omega+3k^2v_{\mathrm{Te}}^2+\omega_{\mathrm{pe}}^2+\Omega_{\mathrm{e}}^2\sin^2\theta\right)+\Sigma\right\}n_{\mathrm{k}}\\&=+i\Sigma_1\left(\omega_0^2+\upsilon_{\mathrm{e}}^2\right)\frac{1-\Omega_{\mathrm{e}}^2/\left(\omega+i\upsilon_{\mathrm{e}}\right)^2}{1-\Omega_{\mathrm{e}}^2\cos^2\theta/\left(\omega+i\upsilon_{\mathrm{e}}\right)^2}n_{\Delta\mathrm{k}}\end{aligned}\tag{17}$$

$$\begin{aligned}&\left[-\Delta\omega\left(\Delta\omega+i\upsilon_{\mathrm{i}}\right)+k^2c_{\mathrm{s}}^2+\frac{m_{\mathrm{e}}}{m_{\mathrm{i}}}\Sigma\right]n_{\Delta\mathrm{k}}=\\&i\frac{m_{\mathrm{e}}}{m_{\mathrm{i}}}\Sigma_1\left\{\omega_{\mathrm{pe}}^2-\left(\omega_0^2+\upsilon_{\mathrm{e}}^2\right)+\left(\Delta\omega+i\upsilon_{\mathrm{e}}\right)\left(\omega_0-i\upsilon_{\mathrm{e}}\right)\right\}n_{\mathrm{k}}\end{aligned}\tag{18}$$

where $\Sigma_1=e\left(\vec{k}\cdot\vec{E}_{\mathrm{k}_0}\right)\Big/2m_{\mathrm{e}}\left(\omega_0^2+\upsilon_{\mathrm{e}}^2\right)$, $\Sigma=e^2\left(\vec{k}\cdot\vec{E}_{\mathrm{k}_0}\right)^2\Big/4m_{\mathrm{e}}^2\left(\omega_0^2+\upsilon_{\mathrm{e}}^2\right)$.

From Eq. (17) and Eq. (18), the dispersion relation for PDI can be obtained:

$$\begin{aligned}&\left\{\left(-\omega^2-i\upsilon_{\mathrm{e}}\omega+3k^2v_{\mathrm{Te}}^2+\omega_{\mathrm{pe}}^2+\Omega_{\mathrm{e}}^2\sin^2\theta\right)+\Sigma\right\}\left\{-\Delta\omega\left(\Delta\omega+i\upsilon_{\mathrm{i}}\right)+k^2c_{\mathrm{s}}^2+\frac{m_{\mathrm{e}}}{m_{\mathrm{i}}}\Sigma\right\}\\&=-\frac{m_{\mathrm{e}}}{m_{\mathrm{i}}}\Sigma\frac{1-\Omega_{\mathrm{e}}^2/\left(\omega+i\upsilon_{\mathrm{e}}\right)^2}{1-\Omega_{\mathrm{e}}^2\cos^2\theta/\left(\omega+i\upsilon_{\mathrm{e}}\right)^2}\left\{\left(\omega_{\mathrm{pe}}^2-\omega_0^2-\upsilon_{\mathrm{e}}^2\right)+\left(\Delta\omega+i\upsilon_{\mathrm{e}}\right)\left(\omega_0-i\upsilon_{\mathrm{e}}\right)\right\}\end{aligned}\tag{19}$$

By setting $\omega=\mathrm{Re}\left(\omega\right)+i\gamma$, $\Delta\omega=\mathrm{Re}\left(\Delta\omega\right)+i\gamma$, $\vec{k}=k\hat{z}$, when the growth rate $\gamma=0$, the threshold of PDI in the steady can be written as

$$E_{\mathrm{th}}^2=\frac{4m_{\mathrm{i}}m_{\mathrm{e}}}{e^2k^2\cos^2\theta}\frac{\omega_0^3\Delta\omega\upsilon_{\mathrm{e}}\upsilon_{\mathrm{i}}}{\omega_0^2+\omega_{\mathrm{pe}}^2}\frac{1-\Omega_{\mathrm{e}}^2\cos^2\theta/\omega_0^2}{1-\Omega_{\mathrm{e}}^2/\omega_0^2}\tag{20}$$

where $\Delta\omega=kc_{\mathrm{s}}$.

For the case when pump wave decays into two Langmuir waves with purely growing mode, e.g. when the oscillation two-stream instability, is excited near the reflection height of the pump wave, the two oppositely propagating Langmuir waves and a zero-frequency purely growing mode are excited by the pump wave. The frequency of the Langmuir wave and purely growing mode are set as $\omega=\omega_0+i\gamma$ and $\Delta\omega=i\gamma$, respectively. The threshold expression becomes

$$E_{\mathrm{th}}^2=\frac{2m_{\mathrm{e}}m_{\mathrm{i}}}{e^2\cos^2\theta}\frac{c_{\mathrm{s}}^2\omega_0^2\left(\omega_1^4+\omega_0^2\upsilon_{\mathrm{e}}^2\right)}{\omega_1^2\left(\omega_0^2+\omega_{\mathrm{pe}}^2\right)}\frac{\left(1-\Omega_{\mathrm{e}}^2\cos^2\theta/\omega_0^2\right)}{\left(1-\Omega_{\mathrm{e}}^2/\omega_0^2\right)}\tag{21}$$

when the growth rate γ is 0; where $\omega_1^2=\omega_0^2-3k^2v_{\mathrm{Te}}^2-\omega_{\mathrm{pe}}^2-\Omega_{\mathrm{e}}^2\sin^2\theta$.

2.2.2 Parametric instability near the upper hybrid resonant region

When the right-hand polarized electromagnetic wave plays its role as a pump wave, it can reach an altitude where the upper hybrid frequency equals the pump wave frequency, called 'the upper hybrid resonant height. In this region, the electric field of the ordinary polarized pump wave is $\vec{E}_{\mathrm{p}} = \left(\hat{x} + i\hat{y}\right)\left(E_{\mathrm{k}_0}/2\right)\cos\left(-i\omega_0 t\right)$.

Then the expressions for $\vec{V}_{\mathrm{k}_0}$, $\vec{V}_{\pm\mathrm{k}}$, $\left(\vec{k}\cdot\vec{V}_{\mathrm{k}_0}\right)\cdot\left(\vec{k}\cdot\vec{V}^{*}_{\mathrm{k}_0}\right)$, and $\left(\vec{k}\cdot\vec{V}_{\mathrm{k}_0}\right)\left(\vec{k}\cdot\vec{V}^{*}_{\pm\mathrm{k}}\right)$ reduce to

$$\vec{V}_{\mathrm{k}_0} = i\frac{e\vec{E}_{\mathrm{k}_0}}{2m_{\mathrm{e}}\left(\omega_0 - \Omega_{\mathrm{e}} + i\upsilon_{\mathrm{e}}\right)} \tag{22a}$$

$$\vec{V}_{\pm\mathrm{k}} = \pm\frac{\omega_{\mathrm{pe}}^2\vec{k}}{k^2\left(\omega - \Omega_{\mathrm{e}} + i\upsilon_{\mathrm{e}}\right)}\frac{n_{\pm\mathrm{k}}}{n_0} \tag{22b}$$

$$\left(\vec{k}\cdot\vec{V}_{\mathrm{k}_0}\right)\cdot\left(\vec{k}\cdot\vec{V}^{*}_{\mathrm{k}_0}\right) = \frac{e^2\left(\vec{k}\cdot\vec{E}_{\mathrm{k}_0}\right)^2}{4m_{\mathrm{e}}^2\left[\left(\omega_0 - \Omega_{\mathrm{e}}\right)^2 + \upsilon_{\mathrm{e}}^2\right]} \tag{22c}$$

$$\left(\vec{k}\cdot\vec{V}_{\mathrm{k}_0}\right)\left(\vec{k}\cdot\vec{V}^{*}_{\pm\mathrm{k}}\right) = \pm i\frac{e\omega_{\mathrm{pe}}^2\left(\vec{k}\cdot\vec{E}_{\mathrm{k}_0}\right)}{2m_{\mathrm{e}}k^2\left[\left(\omega_0 - \Omega_{\mathrm{e}}\right)^2 + \upsilon_{\mathrm{e}}^2\right]}\frac{n_{\pm\mathrm{k}}}{n_0} \tag{22d}$$

For a case when the pump wave decays to an upper hybrid wave and a lower hybrid wave near the upper hybrid resonant region of the pump wave. The threshold for $\gamma = 0$ can be written as

$$E_{\mathrm{th}}^2 = \frac{4m_{\mathrm{e}}^2 n_0\upsilon_{\mathrm{e}}\left(\upsilon_{\mathrm{e}} + \upsilon_{\mathrm{i}}\right)}{3\varepsilon_0 k_{\mathrm{b}}T_{\mathrm{e}}k^4}\frac{\omega_0^4}{\omega_{\mathrm{pe}}^2}\left(1 + \frac{m_{\mathrm{e}}}{m_{\mathrm{i}}}\cot^2\theta\right)\left(1 - \frac{\Omega_{\mathrm{e}}}{\omega_0}\right)^2 \tag{23}$$

by setting the frequency of $\Delta\omega = \mathrm{Re}\left(\Delta\omega\right) + i\gamma$, $\omega = \omega + i\gamma$, and $\vec{k} = k\hat{x}$ into Eq. (12) and (13).

When the pump wave excites the oscillating two-stream instability near the O-mode upper hybrid resonant region, the two upper hybrid waves $\left(\vec{k}_{\pm} = \pm k\hat{x}, \omega_{\pm}\right)$ and a field-aligned purely growing mode $\left(\Delta\vec{k} = -k\hat{x}, \Delta\omega = i\gamma\right)$ are involved. In this case, the threshold expression is:

$$E_{\mathrm{th}}^2 = \frac{4n_0k_{\mathrm{b}}\left(T_{\mathrm{e}} + 3T_{\mathrm{i}}\right)\left(\omega_{\mathrm{pe}}^2 + 3k^2v_{\mathrm{Te}}^2 + \Omega_{\mathrm{e}}^2 - \omega_0^2\right)}{\varepsilon_0\omega_{\mathrm{pe}}^2\left(1 - \Omega_{\mathrm{e}}/\omega_0\right)^2}\left(1 + \frac{3k^2v_{\mathrm{Te}}^2}{\Omega_{\mathrm{e}}\Omega_{\mathrm{i}}}\right) \tag{24}$$

3. Comparison with experimental observations

In this section, threshold calculations have been performed for different experiments conducted at Tromsø, Norway. The relevant ionospheric parameters are provided by EISCAT website (http://www.eiscat.se/madrigal). The neutral densities and collision frequencies are obtained from NRLMSISE-00 [30] and the geomagnetic field strength is obtained from the International Geomagnetic Reference Field (IGRF11) [31].

Four different experiments are considered as listed in Table 1. The experiments on 19th October, 2012 and 7th July, 2014 operated at daytime, and the experiments on 8th November, 2001 and on 2nd October, 1998 ran at nighttime. All these experiments operated with the different heater wave frequency due to the different ionospheric conditions. The effective radiated powers (ERP) listed in the Table 1 take into account the D-region absorption [32]. Figure 1 illustrates the unperturbed electron temperature and electron density profile for these four experiments, which are obtained from the measurement of the undisturbed ionosphere before the heater was turned on. The experiments were chosen to represent both day and night conditions as well as different background electron temperature and electron density. For example, for the two nighttime experiments, the electron density for the experiment on 2nd October, 1998 is much smaller compared to the experiment conducted on 8th November, 2001; whereas the electron temperature is 50% higher in 2nd October, 1998 experiment compared to the experiment on 8th November, 2001. The two daytime experiments of 19th October, 2012 and 7th July, 2014 show similar difference in the electron density and temperature, i.e. higher electron density with lower electron temperature. In the interaction region, the background electron density and electron temperature in the nighttime experiments are lower than in the daytime as expected. Therefore, those four

experiments provide different conditions to calculate the PI threshold as indicated in Table 1 and Figure 1. The unperturbed ionospheric parameters for these four experiments, with aid of NRLMSISE-00 and IGRF model, were used to calculate the threshold and the equivalent ERP of parametric instability as presented in the last eight rows in Table 1. The wave number in the calculation is taken as 12.44π, which is twice the wave number of the 930 MHz UHF radar at Tromsø.

Table 1 The experiments setting and PI threshold

		Data of Experiment			
		19th Oct, 2012	7th Jul, 2014	8th Nov, 2001	2nd Oct, 1998
Time		12:20 - 13:02 UT	9:00 - 12:00 UT	15:15 - 17:30 UT	18:00 - 22:00 UT
Heater wave frequency (f_0)		7.953 MHz	6.710 MHz	6.200 MHz	4.040 MHz
ERP		0.6, 2.1, 4.9, 10.5, 26.3, 52.3 and 104.5 MW	10.5 MW	565 MW	120 MW
Polarization		O-Mode	O-Mode	O-Mode	O-Mode
Heating Cycle		1 min on/ 1 min off	1 min on/ 1.5 min off	2 min on/ 2 min off	8 min on/ 7 min off
PDI near reflection height	Threshold	0.1460 V/m	0.1045 V/m	0.1074 V/m	0.056 V/m
	Equivalent ERP	17.2 MW	10.7 MW	11.2 MW	4.0 MW
OTSI near reflection height	Threshold	0.4155 V/m	0.2678 V/m	0.3559 V/m	0.1653 V/m
	Equivalent ERP	92.4 MW	45.9 MW	81.5 MW	23.1 MW
PDI near the upper hybrid resonant region	Threshold	0.7523 V/m	0.2703 V/m	0.4153 V/m	0.0724 V/m
	Equivalent ERP	300.0 MW	44.7 MW	109.6 MW	3.9 MW
OTSI near the upper	Threshold	0.2788 V/m	0.1572 V/m	0.2454 V/m	0.1036 V/m

hybrid resonant region	Equivalent ERP	41.3 MW	15.1 MW	38.3 MW	8.1 MW

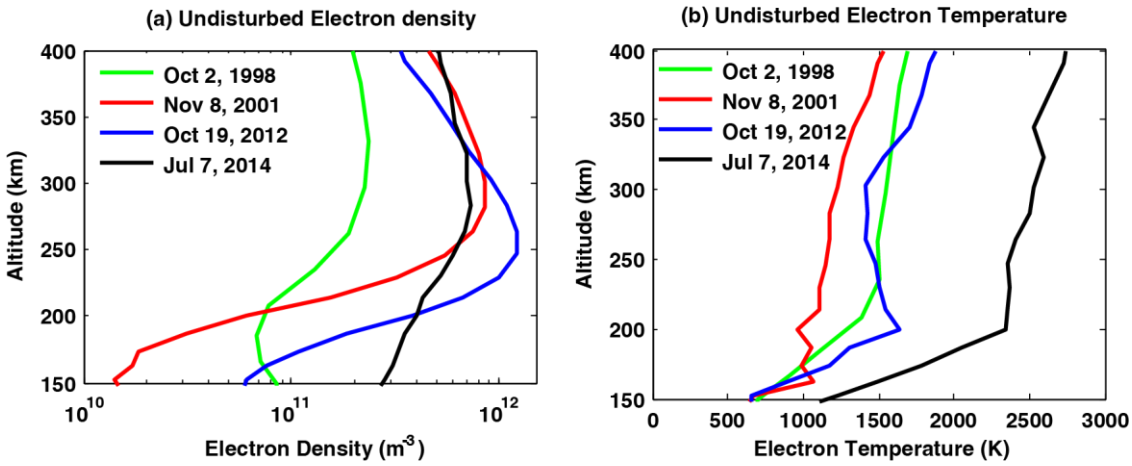

Figure 1. (a) undisturbed electron density profile, and (b) undisturbed electron temperature profiles during the Ionospheric modification experiments; the different colors indicate the different experiments.

For the experiment on 19th Oct, 2012, the downshifted HFILs which indicate the excitation of PDI appear in the ion line spectral when the ERP reached 26.3 MW and the zero-offset HFILs shows when ERP achieved 52.3 MW, which is the signature of the OTSI [33]. Therefore, indicating that the PDI can be excited when the ERP range is from 10.5 MW to 26.3 MW; and the ERP of the excitation of OTSI is within a range of 26.3 MW to 52.3 MW. The lack of observation of HFILs in the ion spectral for 7th July 2014 experiment indicates that the parametric instability was not excited, and there was no obvious heating effect in this experiment. The lack of the PI excitation and heating can be explained by the presence of high electron density in the E-region and consequent high absorption of the pump wave power before reaching the interaction height. The two nighttime experiments displayed intense airglow enhancement and HFILs in the ion line spectra manifesting the excitation of the parametric instability [34, 35].

When the parametric instability is excited near the pump wave reflection height, the threshold of PDI requirement is easy to satisfy in the heating experiments whereas the OTSI requires about

2 times higher threshold than PDI. Both these threshold values for PDI and OTSI are well within the ERP that can be achieved by the Tromsø heating facility. The threshold depends on the effective collision frequencies of charged particles, electron density and electron and ion temperature. Thus, the difference in the PDI threshold for the experiment on 7th July, 2014 compared to the experiment on 19th October, 2012 is due to the difference in electron temperature. As it can be seen from Figure 1, the background electron temperature was high during the experiment of 7th July, 2014, resulting in a high threshold value. The effective collision frequencies of the electron and ion decrease with the growth of the temperature which significantly influences the threshold value. The difference of the thresholds in the nighttime experiments compared to the daytime experiments can also be explained due to the electron temperature difference.

When the parametric instability occurs near the pump wave upper hybrid resonant region, the threshold is related to the wavelength of the plasma wave, which is associated with the transvers width of the irregularities. The backscatter UHF radar cannot detect the upper hybrid waves excited by the parametric instability; thus, in this paper, it's assumed that the wave number of upper hybrid wave is twice the wave number of the 930 MHz UHF radar. The threshold of parametric instability is considerably influenced by the scale of the irregularities, due to the relation between wavelength and wave number $k = 2\pi/\lambda$.

3.1 Comparison with other PDI threshold calculation reported in the literature

The results presented in section 2 are compared with the results presented in Kuo's paper [7]. The relevant parameters of the HF heating experiments conducted at Tromsø, Norway have been used for the threshold calculation as given below: $\Omega_e/2\pi = 1.35$ MHz , $T_e = 1500$ K ,

$T_i = 1000$ K , $\upsilon_{in} = 0.8$ s^{-1} , $v_{Te} = 1.5\times10^5$ m/s , $v_{Ti} = 7.17\times10^2$ m/s , $c_s = 1.52\times10^3$ m/s , $\upsilon_{iL} = 1.19\times10^4$ s^{-1} , $\upsilon_e = 600$ s^{-1} , $\theta = 12^\circ$. The threshold values estimated by Eq. (20) and (21) in this paper are compared to Eq. (21) and Eq. (25) in Ref. 7 and listed in the Table 2.

Table 2. Comparison of the threshold evaluations

Equations	$\omega_0/2\pi = 5.423$ MHz	$\omega_0/2\pi = 6.77$ MHz
Eq. (21) in Ref. 7 $E^2_{OTSIth} = \frac{2m_e m_i}{e^2\cos^2\theta} c_s^2 \omega_0 \upsilon_e$	0.44 V/m	0.49 V/m
Eq. (21) $E^2_{th} = \frac{2m_e m_i}{e^2\cos^2\theta} \frac{c_s^2\omega_0^2\left(\omega_1^4+\omega_0^2\upsilon_e^2\right)}{\omega_1^2\left(\omega_0^2+\omega_{pe}^2\right)} \frac{\left(1-\Omega_e^2\cos^2\theta/\omega_0^2\right)}{\left(1-\Omega_e^2/\omega_0^2\right)}$	0.31 V/m	0.34 V/m
Eq. (26) in Ref. 7 $E^2_{PDIth} = \frac{4m_e m_i \upsilon_e \upsilon_i \omega_0^3 \Delta\omega}{e^2k^2\omega_{pe}^2\cos^2\theta} \frac{1-\Omega_e^2\cos^2\theta/\omega_0^2}{1-\Omega_e^2/\omega_0^2}$	0.27 V/m	0.3 V/m
Eq. (20) $E^2_{th} = \frac{4m_i m_e}{e^2k^2\cos^2\theta} \frac{\omega_0^3\Delta\omega\upsilon_e\upsilon_i}{\omega_0^2+\omega_{pe}^2} \frac{1-\Omega_e^2\cos^2\theta/\omega_0^2}{1-\Omega_e^2/\omega_0^2}$	0.14 V/m	0.16 V/m

As illustrated in Table 2, the PDI threshold value near the pump wave reflection height calculated by the equations in Kuo's paper [7] are higher by nearly a factor of 2 compared to our results; also, for the OTSI, Kuo's result is approximately 1.4 times more than the threshold values obtained using the derived equations in this paper. For the experiment performed on 19th October 2012, the Langmuir PDI had been excited when ERP reached 26.3 MW; but 10.5 MW ERP cannot excite parametric decay instability, i.e. the equivalent ERP of the threshold value range of PDI is from 10.5 MW to 26.3 MW. We have calculated the PDI threshold value and equivalent ERP using Eq. (21) are around 0.15 V/m and 17.2 MW, shown in the Table 1, as well as Eq. (26) in Kuo 2015

paper [7]. The threshold of PDI using Eq. (26) in Kuo's paper [7] is 0.204 V/m and the equivalent ERP is 33.7 MW, which are higher than the experimental observation.

4. Summary

In the present study the excitation of plasma waves due to high-frequency electromagnetic wave heating in the ionosphere are discussed. Equations that describe the threshold field of pump waves for the excitation of parametric instability have been derived. The results are also compared with the experiments operated with EISCAT heating facility. Our study indicates that the threshold field of the excited parametric instability is proportional to the product of the electron collisions frequency and the ion collisions frequency, including the effects of the Landau damping, which plays important roles in the threshold estimation. Our results also demonstrate that the OTSI requires higher threshold than PDI, which is consistent with the experimental observations. In the dispersion relation of the excited high frequency sideband and low frequency decay mode, the coupling terms in right hand side of Eq. (12) and Eq. (13) drive the excited plasma wave modes. The first term of the right-hand side arises from the spatial non-uniformity of the high frequency wave, which cannot be neglected in the excitation process. Therefore, using the threshold expression derived in this paper and comparing with results of previous research as indicated in Table 2 illustrates that the inclusion of the inhomogeneity of the pump wave field are important and need to be considered when evaluating the threshold of PDI in order to explain experimental observations.

Acknowledgments

EISCAT is an international scientific association supported by research organizations in China (CRIRP), Finland (SA), Japan (NIPR and STEL), Norway (NFR), Sweden (VR), and the

United Kingdom (NERC). This work was supported by the National Natural Science Foundation of China (NSFC grants 41204111, 41574146, 41774162 and 41704155) and China Postdoctoral Science Foundation (2017M622504). The data used in this paper are available through the EISCAT Madrigal database (http://www.eiscat.se/madrigal/).

References

[1] Utlaut W F and Cohen R 1971 *Science* **174** 245

[2] Grach S M and Trakhtengerts V Y 1975 *Radiophys. Quantum El*. **18** 951

[3] Minkoff J *et al* 1974 *Radio Sci* **9** 941

[4] Robinson T R 1989 *Phys. Rep*. **179** 79

[5] Stubbe P 1996 *J. Atmos. Terr. Phys.* **58** 349

[6] Leyser T B and Wong A Y 2009 *Rev. Geophys.* **47** 514

[7] Kuo S P 2015 *Phys. Plasmas* **22** 012901

[8] Frey A 1986 *Geophys. Res. Lett.* **13** 438

[9] Rietveld M T *et al* 2000 *J. Geophys. Res.* **105** 7429

[10] Bernhardt P A *et al* 1989 *J. Geophys. Res.* **94** 9071

[11] Kosch M J, *et al* 2002 *Geophys. Res. Lett.* **29** 27

[12] Kosch M J *et al* 2007 *J. Geophys. Res.* **112** A06325

[13] Stubbe P *et al* 1984 *J. Geophys. Res.* **89** 7523

[14] Thome G D and Blood D W 1974 *Radio Sci.* **9** 915

[15] Frolov V L *et al* 2014 *Radiophys. Quantum El.* **57** 393

[16] Perkins F W *et al* 1974 *J. Geophys. Res.* **79** 1478

[17] Fejer J A 1979 *Rev. Geophys.* **17** 135

[18] Kuo S P 1996 *Phys. Plasmas* **3** 3957

[19] Kuo S P 2014 *Pr Electromagn Res.* **60** 141

[20] Kuo S P *et al* 1983 *J. Geophys. Res.* **88** 417

[21] Gekker I R 1982 The interaction of strong electromagnetic fields with plasmas *Clarendon Press* Oxford

[22] Silin V P 1965 *Sov. Phys. JETP* **21** 1510

[23] Silin V P 1968 *Proc. Eighth Int. Conf. Phenom Ionized Gases* 205

[24] Nishikawa K 1968 *J. Phys. Soc. Jpn*. **24** 916

[25] Nishikawa K 1968 *J. Phys. Soc. Jpn.* **24** 1152

[26] Fejer J A and Leer E 1972 *J. Geophys. Res.* **77** 700

[27] Guzdar P N *et al* 1996 *J. Geophys. Res.* **101** 2453

[28] Tzoar N 1969 *Phys. Rev.* **178** 356

[29] Utlaut W F and Violette E J 1972 *J. Geophys. Res.* **77** 6804

[30] Picone J M *et al* 2002 *J. Geophys. Res.* **107** 1468

[31] Finlay C C *et al* 2010 *Geophys. J. Int.* **183** 1216

[32] Senior A *et al* 2010 *J. Geophys. Res.* **115** A09318

[33] Bryers C J *et al* 2013 *J. Geophys. Res.* **118** 7472

[34] Blagoveshchenskaya N F *et al* 2005 *Ann. Geophys.* **23** 87

[35] Bryers C J *et al* 2012 *J. Geophys. Res.* **117** A09301